Demonstrating Shock Mitigation and Drag Reduction by Pulsed Energy Lines With Multi-domain WENO

Kevin Kremeyer[1], Kurt Sebastian[2] and Chi-Wang Shu[3]

ABSTRACT

A series of numerical experiments were performed in which energy was deposited ahead of a cone traveling at supersonic/hypersonic speeds. The angle of attack was zero, and the cone half-angles ranged from 15-45 degrees. The Mach numbers simulated were 2, 4, 6, and 8. The energy was deposited instantaneously along a finite length of the cone axis, ahead of the cone's bow shock, causing a cylindrical shockwave to push air outward from the line of deposition. The shockwave would sweep the air out from in front of the cone, leaving behind a low-density column/tube of air, through which the cone (vehicle) propagated with significantly reduced drag. The greatest drag reduction observed was 96% (100% drag reduction would result in the complete elimination of drag forces on the cone). The propulsive gain was consistently positive, meaning that the energy saved due to drag reduction was consistently greater than the amount of energy "invested" (i.e. deposited ahead of the vehicle). The highest ratio of energy-saved/energy-invested was approximately 6500% (a 65-fold "return" on the invested energy). We explored this phenomenon with a high order accurate multi-domain weighted essentially non-oscillatory (WENO) finite difference algorithm, using interpolation at sub-domain boundaries. This drag-reduction/shock-mitigation technique can be applied locally or globally to reduce the overall drag on a vehicle.

Key Words: energy deposition, shock mitigation, axisymmetric Euler equations, WENO finite difference method, multi-domain, supersonic/hypersonic, flow control, drag reduction.

[1]Associate Fellow AIAA; Vice President of Research, PM & AM Research (AIAA Corporate Member), Tucson, AZ 85719; E-mail: kremeyer@physics-math.com

[2]Member AIAA; Associate Professor, Department of Mathematics, U.S. Coast Guard Academy, New London, CT 06320; Visiting Research Scholar, Brown University; E-mail: ksebastian@exmail.uscga.edu

[3]Professor, Division of Applied Mathematics, Brown University, Providence, RI 02912; E-mail: shu@dam.brown.edu. Research of this author was supported by ARO grant W911NF-04-1-0291, NSF grant DMS-0207451 and AFOSR grant FA9550-05-1-0123.

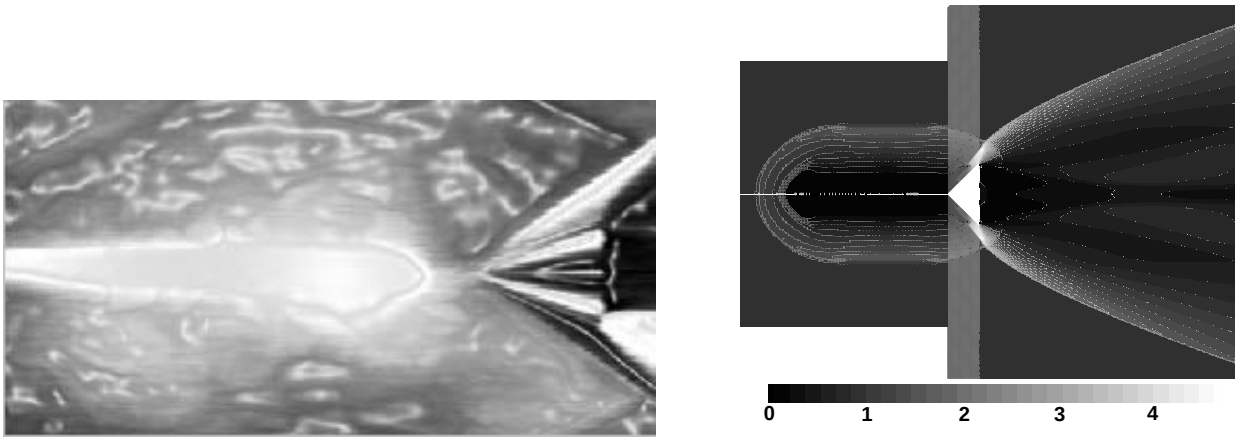

Figure 1.1: Qualitative and numerical experiments for pulsed energy line deposited before a supersonic cone. An extended path is heated ahead of a cone in a supersonic flow. Left: wind tunnel experiment. Right: numerical simulation showing density contours.

1 Introduction

The objective of this paper is to describe and characterize a flow-control/drag-reduction method for supersonic/hypersonic flight. The initial investigation of this technique was experimental and the data obtained was mainly qualitative. We have numerically performed many similar experiments using a multi-domain weighted essentially non-oscillatory (WENO) finite difference method developed in [34] to compute the three-dimensional axisymmetric Euler equations. The robustness and validation of this method for recognized test cases is demonstrated extensively in [34]; however, this current example is the first time calculations of this geometric complexity were computed using a high order finite difference method. To our knowledge, simulation for this specific problem has not been performed before. Therefore, there are no known reliable sources, against which to compare the results, other than qualitative experimental results, such as schlieren photographs (an example of which can be seen in Figure 1.1) and coarse pressure measurements at the cone. Qualitative similarity of the experimental and computed images and pressures indicate the validity of our numerical technique.

2 Energy deposition in supersonic flows

2.1 Motivation for the experiments

Hypersonic and supersonic vehicles generate shock waves, which are accompanied by a host of technical challenges. These include increased drag, sonic boom, and destructively high temperatures and pressures on both airframe and components. "Suddenly" (as opposed to "gently") heating an extended path of air, ahead of the shock wave and along the vehicle's velocity vector, results in rapid expansion of the heated air. This creates a long, hot, low-density core, into which the vehicle's bow shock expands, followed by the vehicle itself (see again Figure 1.1). Strategically heating extended regions of gas ahead of the vehicle can therefore mitigate the shock wave, as well as its deleterious effects. Also, since the vehicle will preferentially fly along the low-density channel, (i.e. be partially steered by it), adjusting the direction of hot core formation can be utilized as a method of control. The benefits of this technology therefore include tremendous increases in fuel efficiency and control, which remain outstanding problems in all supersonic/hypersonic platforms.

In addition to drag reduction and flow control, effective shock wave mitigation will also decrease ablation/heat resistance requirements of critical surfaces and components. The potential result is therefore faster, more durable/maneuverable systems, with increased kinematic footprints. Our calculations and simulations predict a reduction in wave drag of more than 90%, with a return ratio (defined as the ratio of the thrust (power) saved over the invested power) of ∼10:1 for a streamlined body and ∼65:1 for a bluff body. The electromagnetic nature of this technology addresses the desire to move away from complex actuator systems and control surfaces, while the technology's non-mechanical ability to "streamline" arbitrary bodies addresses the desire to reduce both time and cost of design, development, and maintenance. It allows manufacturers to approach the ideal situation of designing an airframe around its payload and mission, while depending on an electro-optic system to take care of the "stream-lining" for them. A very long, low-density path, opened up ahead of an airframe, will provide any vehicle with a much more favorable "effective aspect ratio",

allowing it to propagate through the low-density tube, with greatly-reduced resistance.

The potential benefits of this technology span the applications of high-speed flight. Reducing drag reduces fuel requirements and therefore translates directly into lower weight and/or greater range/payload. Furthermore, the associated reduction in heating/pressure translates into less stringent materials requirements, less damage, and/or increased performance envelopes. A third major benefit is the decreased environmental (acoustic) impact of high-speed vehicles, in the form of sonic boom mitigation. The combination of all of these benefits stands to increase kinematic footprint through greater speed and range with a lower acoustic signature.

In the past, air has been "pushed" laterally out of the way of a moving vehicle by using an aerospike. The approach described here offers the possibility of pushing air laterally out of a vehicle's way, tens, even hundreds of meters ahead of the vehicle. This method is all the more alluring, because the "pushing" is performed without the impediment of a physical spike, which can actually become a liability when the vehicle is moving at a non-optimized angle of attack.

Another benefit is apparent in applying this technology to develop a new maneuvering (control) method, which is more efficient at higher Mach numbers. This approach represents an excellent opportunity for us to overcome the problems of the supersonic implementation of traditional control methods, which have oftentimes evolved from subsonic applications. An example of localized flow control using energy deposition is the mitigation of detrimental effects of a shock/shock interaction on an air vehicle during maneuver. Shock/shock interactions can occur on supersonic and hypersonic aircraft during maneuver and sustained flight. For example, oblique shock waves propagating from the nose of an aircraft or missile can interact with the bow shock of any body protruding from the fuselage, e.g. stabilizing fins, external payloads, booster rockets, engine cowls, and inlets. Some shock/shock interactions can lead to severe and often catastrophic events for aircraft.

2.2 Past work

Shockwaves have traditionally been studied and characterized during propagation through a medium, free of fluctuations over length scales characteristic of the driving body. More recently, however, the investigation of such disturbances has become increasingly common. In fact, the last decade has seen an increased interest in controlling/mitigating shockwaves by modifying/controlling the gas ahead of them. Historically, one of the first attempts to do this was with a long, thin spike at the tip of the vehicle. Such an aero-spike generally protrudes well ahead of the vehicle nose, creating its own shockwave, and significantly reduces the drag on the vehicle. This technique is still being investigated, e.g. by Guy et al. [10]. Other mechanical methods of affecting the shockwave have also been researched over the decades, including counter-propagating streams of:

- gas (Kandebo [15] and Yudintsev et al. [37])
- heated/reacting/ionized gas (Shang et al. [35])
- liquid (e.g. water)

and even using an ablative aero-spike (e.g. Teflon^{TM}) to deposit its degradation products into the flow.

The benefits of these methods have typically been reported when applied to bluff bodies, and all have reported drag reduction as high as 50%. One complaint of such reported benefits is that they often merely approach the savings which can be achieved by using a more aerodynamic body. Another problem is that all of the "counterflow" methods are similar to the solid/rigid aero-spike, in that they also physically push forward against the air. As a result, these methods also suffer from the fundamental mechanical limitation of forming their own shock wave, i.e. they are unable to "get ahead" of a shock.

An intuitive means to circumvent this limitation is to use electromagnetic radiation to affect the air ahead of a shock. This has also been investigated over the past several decades.

One of the initial electromagnetic methods investigated was to ionize the gas ahead of the shockwave. This was accomplished in a number of different ways, including RF and DC plasmas (Klimov et al. [16] and Ganguly et al. [9]). For years, the observed effects had commonly been attributed to an interaction of electrons/ions with the shockwave. However, further fluid simulations (Kremeyer et al. [17, 18, 19], Riggins et al. [29], and Hilbun et al.[4]) led to gradual acceptance that the primary factor in the observed dynamics is thermal. Experimental reports then began to concur (Merriman et al. [25] and Ionikh et al. [13]). Despite this more balanced understanding, there do remain finer effects of ionization, which continue to be investigated (Bityurin et al. [4] and Bletzinger et al. [5]).

In the course of numerically investigating shock propagation through various density and temperature profiles, Kremeyer et al. [20] noted the increased shock speed and decreased pressure jump experienced when a shockwave encountered a heated swath of gas. The most dramatic effect, by far, was obtained when the swath (strip) was aligned with the direction of shock propagation (resulting in the shock making a "T" with the heated swath of gas). The effect was present even for a very narrow strip, and it was strongest when the temperature in the strip was highest. Due to the higher speed of sound within the hot swath, the most apparent feature was for the shock to bulge forward as it propagated into the heated region. The pressure jump across the "bulged" region of the shock was also lowered. In general, when propagating into a time-invariant and relatively moderate temperature cross-section, the shock structure adopts a steady shape and constant speed. Behind the shock, a flow pattern establishes itself to allow the steady shape to persist and to continue propagating. In contrast, a much more dramatic effect is observed when the swath is sufficiently heated (yielding a high enough speed of sound) to effectively eliminate the local pressure jump. (In a practical sense, this occurs when the speed of sound in the heated swath is greater than the vehicle speed.) In this case, the shock is effectively "punctured", allowing the high-pressure fluid (formerly fully-contained behind the shock) to flow freely forward along the hot path.

[4]W. Hilbun and W. Bailey, (AIFT), private communication, 1997.

This creates a forward-propagating, low-density jet, along which the more highly compressed neighboring fluid (behind the "unpunctured" shock) can be entrained and escape forward as well. Creating such a strongly heated swath ahead of the bowshock of a supersonic vehicle therefore allows a release of the high-pressure gas behind the shockwave. This effect can be exploited to strategically reduce the local drag/pressure on the vehicle to aid in maneuvering. For the greatest overall drag reduction, a path can be heated along the vehicle's stagnation line.

Providing a mechanism to help realize the desired energy-deposition geometries, ultrashort laser technologies can use laser radiation to produce extended swaths of hot, ionized gas. Typically, when an energetic laser is focused to a point to ionize air, the resulting plasma disperses the beam/pulse. In a large parameter range, however, high energy pico- and femto-second laser pulses have actually been found to propagate over large distances, while heating and ionizing gas in their path. This phenomenon is referred to as filamentation (Diels et al. [7]). It has also been observed using: wavelengths ranging from the IR to UV (Schwarz et al. [32]); pulse durations from picoseconds to tens of femtoseconds; and pulse energies from milliJoules to Joules. Spatially, the filamenting pulses have been reported to extend over hundreds of meters, and the filament diameters have been reported to range from 0.1 to several millimeters (La Fontaine et al. [22], Brodeur et al. [6]). The laser pulse can be focused and adjusted to control the point at which filamentation begins and ends, and the rapid expansion due to the gas-heating can result in an audible "crack" or "snap". Current work indicates that ionized filaments, which propagate over kilometers, can be obtained with nanosecond UV lasers, given sufficient pulse power/energy (Schwarz et al. [33]).

In response to the above observations and developments, a number of implementations have been developed to take advantage of this novel geometry [21]. Some of these implementations involve the use of laser pulses to heat the gas ahead of the shockwave. The use of lasers to heat the air ahead of a shockwave is not new (Adelgren et al. [1], Myrabo et al. [26], Aleksandrov et al. [2]). However, the methods investigated in the past were

not capable of creating a long narrow path of heated gas which can be scaled up to large dimensions (e.g. heated paths hundreds of meters long). Past laser-heating methods have primarily depended on focusing their energy to a point ahead of the shockwave. These can generate slightly extended regions of hot/ionized gas, but not the long paths required for optimal pressure release. To achieve long, ionized paths, one can use a number of methods, including weakly focused UV pulses and filamenting lasers. To further increase the energy deposition, bundles of filaments can be used, or an electric discharge can be guided along the laser-ionized path (Rambo et al. [28]). This technique provides a very efficient method of quickly heating a line of air. The rapidly deposited energy of such heating methods not only creates a low-density swath of gas, but also results in the necessary cylindrical shockwave propagating outward from the orignially heated path (described in the next section).

As the vehicle moves forward into the heated swath, the cylindrical shockwave continues to propagate outward. Therefore, the vehicle sees a gradually widening low-density region with its enveloping cylindrical shockwave expanding outward (the cylindrical shockwave eventually degrades to a soundwave due to the expansion). The air left inside of the expanding cylindrical shockwave remains elevated to a higher temperature, with a lower density and higher speed of sound than the original ambient air. This residual or "ancillary" heating has been meticulously characterized by Plooster [27], and yields the drag reduction benefits investigated in this paper. The net heating on an air frame when propagating through this higher-temperature, lower-density core is greatly decreased from the temperatures that would result from propagating through full-density, lower-temperature air.

2.3 Creating a low-density core

Over the decades, the evolution of large amounts of energy concentrated along point and line sources have been thoroughly characterized (Schreier [31], Plooster [27], Sachdev [30], and Lutzky et al. [24]). In his meticulous computational study, Plooster [27] provides his data in dimensionless units for an infinite line source of energy. In all of his graphs, the energy

is deposited at $r = 0$, and the distance from this origin (in one-dimensional cylindrical coordinates) is described using the dimensionless radius λ. In each graph, λ is plotted along the abscissa, and it represents the ratio of the true distance r to a characteristic radius $R_0 = (E_0/b\lambda p_0)^{1/2}$, where E_0 is the energy deposited per unit length, p_0 is the pressure ahead of the shock, $\lambda = 1.4$ and b is taken to be 3.94. Several plots are drawn on each graph, with numbers above each individual line. These numbers represent the dimensionless time τ, which is the ratio of the real time t to a characteristic time $t_0 = R_0/a_0$, where a_0 is the speed of sound in the ambient atmosphere ahead of the shockwave.

Additional utility of these results comes from the fact that Plooster verified them for a variety of initial conditions. The long-term dynamics (of interest to us) are basically identical for initial conditions ranging from ideal line-sources, to more diffuse sources. The results are presumably robust enough to further encompass any method we can conceive to deposit energy along an extended region ahead of the shockwave we would like to mitigate/control.

As the shockwave propagates radially outward, a rarefaction begins to develop behind the expanding shockwave at approximately $\tau = 0.2$. This ultimately results in a reversed flow at approximately $\tau = 0.56$ when the gas near this rarefaction begins to flow back toward the origin, instead of continuing to flow outward.

It is at this point of flow-reversal that the most important feature of these dynamics becomes "locked in." From approximately $\tau = 0.56$ to well beyond $\tau = 6.0$, a very low density core, within the expanding cylinder of air, remains effectively stationary and unchanged from $\lambda = 0$ to approximately $\lambda = 0.5$. The beauty and utility of this arbitrarily long, low-density cylindrical core is that it persists for a very long time and can be used as a low-density channel, through which a vehicle (and/or the high-pressure air being pushed by it) can travel. Thermal diffusion is far too slow to significantly alter the core before the vehicle passes through it.

The parameters and scales from Plooster's results were used to estimate the energy/power requirements for our test cases. The simulations are intended to show the compelling advan-

tage in shock-mitigation and drag-reduction when suddenly depositing heat along a streamline ahead of a shockwave. The sustained benefit, demonstrated in the line-deposition geometry, results in extended periods of shock-mitigation/drag-reduction, without continual energy addition. This allows the heating mechanism to be operated in a pulsed mode. Once the energy is deposited, a long path of air is heated. This path expands according to the dynamics reported by Plooster [27]. His results show that the internal low-density core (which we would like to exploit) is fully developed by approximately $\tau = 0.34$ and is usable until at least $\tau = 6.0$.

2.4 General energy estimates

Given the above considerations of Plooster, we can make rough estimates of the energy required per pulse for effective shock-control/drag-reduction. Such rough considerations take only into account the low density core ahead of the vehicle. Two neglected "nonlinear" effects are the fluid's lateral velocity, and the "recirculation pressure" behind the vehicle. As a result of the high density air channeled around the vehicle, the pressure behind it actually has the potential to be raised, resulting in not only a low-density channel for the vehicle to propagate into, but also a higher pressure behind the vehicle to help push it forward. A more encompassing analysis requires much more careful simulations and experiments to investigate these full effects. Our first step in this direction has been to perform the simulations using a multi-domain high order accurate WENO finite difference CFD code developed in [34]. An in-depth explanation of this effort can be found in the section 4 of this paper on numerical results. Our next step will be to conduct wind tunnel experiments with precise, high-resolution diagnostics.

The standard feature which we will use to discuss the aerodynamic benefit is the low-density core, which Plooster showed to extend to approximately $\lambda = 0.5$ (Figure 4 in [27]). If we would like the radius of this core to be $\frac{1}{2}$ of the vehicle radius, we can calculate the necessary energy deposition per length (E_0) using the definition of $\lambda = r/R_0$, where

$R_0 = (E_0/5.34 * p_0)^{\frac{1}{2}}$ and p_0 is the ambient air pressure. This gives us the energy per length necessary to create a low-density core of radius r. First we rearrange to get $E_0 = 5.34 * p_0 * R_0^2$. Then, expressing R_0 in terms of λ and r, we obtain: $E_0 = 5.34 * p_0 * (r/\lambda)^2$. The main value of λ, about which we care, is $\lambda = 0.5$, because this is the approximate dimensionless width of the low-density core. A primary dimension, which provides us with physical information, is the actual radius r of the low-density core we would like to create. As can be expected, the energy per length required to create a given low-density core is proportional to the square of its radius (i.e. proportional to its cross-sectional area) $E_0 = 21.5 * p_0 * r^2$. To obtain the total energy required, we must simply multiply E_0 by the length of the heated path. This length is one of the system parameters that must be investigated in the testing phase, and it also plays a role in determining the pulse repetition rate (which will also be investigated during testing). However, one can choose nominal values in order to estimate ranges of pulse energy and average power.

One approach of heating the gas ahead of a vehicle is to prevent "breaks" in the hot path by creating each new low-density "core" so that its front end is butted up against the preceding core's back. However, one possible way to save on power and total energy deposition is to leave a break of unheated air between the successive individual cores. This will allow us to exploit some of the time required for the shockwave to actually re-form ahead of the vehicle. As the vehicle's shockwave is re-forming, the next heated core will break it up again. Bruno et al.[5] demonstrated this phenomenon in spot-heating ahead of a vehicle. In practice, the optimal ratio of the hot-core length to the unheated length will have to be determined with wind tunnel tests and additional detailed simulations.

3 Heating/shockwave interaction: past work

The reason for discussing the above method(s) to heat an extended path of air is its direct applicability to the control/mitigation of a shockwave. We will begin by recalling time-resolved

[5] C. Bruno et al., private communication, 1995.

studies of point-heating in front of a shockwave, then we will summarize the experiments we have performed in the past with regions of extended heating.

The beautiful time-resolved windtunnel studies of Adelgren et al. [1] allowed the observation of energy-deposition effects on a spherical shockwave at Mach 3.45. The region of laser heating is approximately a point source; however, it is somewhat elongated along the direction of laser-pulse propagation, which occurs transverse to the tunnel's air-flow (the beam enters from the side of the tunnel). The resultant heating can effectively be approximated as a point source, whose evolution as an expanding spherical shockwave has been extensively treated (Sachdev [30], Lutzky et al. [24]). The main signature of this expansion is the spherical shockwave driving a high density/high pressure wave outward, leaving a hot, low-density "bubble" in the center. This low-density "bubble" expands to a point and then stops, as the shockwave continues outward and weakens.

To investigate the more effective cylindrical geometry, experiments were performed, in which a line of gas was heated, ahead of a model, along a streamline (Figure 1.1). Although the flow was not thoroughly characterized, several milestones were achieved and qualitative observations were made.

- Geometries were implemented in the wind tunnel to add heat along a streamline, both "gently" and "suddenly".
- Aspects of drag-reduction due to sudden heating along a streamline were inferred through a quantitative study of gentle heat injection.
- A laser-guided/initiated high-voltage discharge was demonstrated in the windtunnel, as a method to scale up energy addition along the path of a filamenting laser.
- A fundamental study was performed to help implement laser-guided discharges over a large range of vehicle operating pressures.
- A schlieren study indicated a strongly weakened bowshock, due to the laser-guided/initiated electric discharge.

The results of this study indicated strong overall drag-reduction and shock-mitigation through sudden heat addition along a streamline ahead of a shock wave. The method was inferred to result in significant energy savings and was anticipated to apply to both streamlined and bluff bodies. Based on the measurements, an estimate of the drag reduction on a 23-degree (half-angle) cone at Mach 2.45 was approximately 30%. The method was also inferred to help maneuver a vehicle (when applied off of its stagnation line) by providing asymmetric drag reduction (estimated up to 10%).

In addition to the above experimental work, we have also performed analytical calculations and numerical simulations for a shock-tube geometry with a normal shock impinging on a region of deposited energy. These considerations indicated the great advantage of an extended geometry. A given amount of energy was deposited either at a point ahead of the shock wave, or along a line ahead of the same shock wave (oriented in the direction of the shock wave's propagation). The point heating resulted in some mixing of the gas, but the overall impact on the shock was minimal. In terms of a supersonic vehicle, very little air is pushed out of a vehicle's path with a "point-heating" geometry. Nearly half of the gas expands toward the vehicle and impinges "head-on" with the vehicle's shock wave, while the other half moves away from the vehicle, only to be "caught up to" and absorbed by the vehicle's shock wave. In contrast, for the case of sudden line heating, nearly all of the cylindrically-expanding gas is pushed out of the way of the vehicle's path. In fact, a long-lived reduction in density is observed surrounding the heated path, well after the gas is initially heated. It is along this low-density channel or core that the vehicle will travel.

Once the vehicle has fully exploited a heated path (core), another violently heated path can be created, resulting in a repetition rate which is dictated roughly by the vehicle's size and speed, as well as the length of the heated core. To scale the method up beyond a single heated path, arrays of individual heating elements can be implemented. The energy-deposition from these arrays can be phased to maintain strong outward gas expansion, tailored to the size and speed of the vehicle.

4 Numerical results

In order to account for the complex dynamics and shock/shock interactions inherent in this problem, a novel modeling formalism was required to properly simulate the shock dynamics. This method was a multi-domain weighted essentially non-oscillatory (WENO) high-order finite difference method in which interpolation is employed at sub-domain interfaces. WENO schemes were originally designed based on the successful essentially non-oscillatory (ENO) schemes by Harten, Engquist, Osher and Chakravarthy [11]. Finite volume WENO schemes have been constructed by Liu, Osher and Chan [23] for a third order version in one space dimension, by Friedrichs [8] and Hu and Shu [12] for second, third and fourth order versions for 2D general triangulations, and by Shi, Hu and Shu in [36] for high order versions containing negative linear weights. Finite difference WENO schemes have been constructed by Jiang and Shu [14] for the third and fifth order versions in multi-space dimensions with a general framework for the design of the smoothness indicators and nonlinear weights, and by Balsara and Shu [3] for very high order (between 7 and 11) versions. Recently, Sebastian and Shu [34] constructed a multi-domain fifth order WENO finite difference scheme of which the numerical simulations described in this paper comprise.

4.1 Multi-domain WENO finite difference algorithm

Both ENO and WENO use the idea of adaptive stencils in the reconstruction procedure based on the local smoothness of the numerical solution to automatically achieve high order accuracy and the non-oscillatory property near discontinuities. ENO uses just one (optimal in some sense) out of many candidate stencils when doing the reconstruction. WENO, on the other hand, uses a convex combination of all the candidate stencils, each being assigned a nonlinear weight which depends on the local smoothness of the numerical solution based on that stencil. WENO improves upon ENO in robustness, better smoothness of fluxes, better steady state convergence, better provable convergence properties, and more efficiency.

There are two types of WENO schemes, namely the finite volume schemes and the fi-

nite difference schemes. In one spatial dimension, the finite volume schemes and the finite difference schemes are equivalent, both in numerical resolution and accuracy and in complexity of coding and CPU timing. For multi-spatial dimensions, however, they are no longer equivalent. While finite difference schemes are still very simple to code and fast to compute (essentially only one or more outside "do loops" are needed to change a one dimensional finite difference code to multi-dimensions), the finite volume code becomes much more complicated and costly. The multi-domain framework employed in our numerical simulations served multiple purposes. To utilize the speedier finite difference framework in this two-dimensional problem, it became necessary to divide the larger domain into three smaller sub-domains to allow for the computation of the complex geometry around the cone-shaped vehicle in flight. These sub-domains can be observed graphically in the figures to follow. The drawback to using this finite difference scheme over several sub-domains is that conservation error is necessarily introduced since interpolation in any manner is non-conservative if it is not based on cell averages. Much time was spent on this "drawback" during the development of the method. Most importantly, it has been proved [34] that under suitable assumptions interpolation does not produce $O(1)$ conservation error. In fact, the method is "essentially conservative" in that the conservation error reduces with reduction in mesh size. Also, many numerical investigations have shown that full high order accuracy is maintained across the global domain and the essentially non-oscillatory results are also maintained even though interpolation is employed at sub-domain interfaces.

4.2 The axisymmetric Euler system in 3D

To compute the type of flow we have described thus far in this paper, the flow is assumed to be governed by the axisymmetric Euler equations in three dimensions. Because the equations are axisymmetric, they reduce to a two dimensional Euler system with an extra equation and some forcing terms on the right hand side. To be specific, the three dimensional axisymmetric

Euler equations reduce to the following two dimensional system:

$$\begin{pmatrix} \rho \\ \rho u_x \\ \rho u_r \\ \rho u_\theta \\ E \end{pmatrix}_t + \begin{pmatrix} \rho u_x \\ \rho u_x^2 + p \\ \rho u_r u_x \\ \rho u_\theta u_x \\ u_x(E+p) \end{pmatrix}_x + \begin{pmatrix} \rho u_r \\ \rho u_x u_r \\ \rho u_r^2 + p \\ \rho u_\theta u_r \\ u_r(E+p) \end{pmatrix}_r = \begin{pmatrix} \frac{\rho u_r}{r} \\ \frac{\rho u_x u_r}{r} \\ \frac{\rho\left(u_r^2 - u_\theta^2\right)}{r} \\ \frac{2\rho u_\theta u_r}{r} \\ \frac{u_r(E+p)}{r} \end{pmatrix} \tag{4.1}$$

where as is common ρ is the density, p is the pressure, (u_x, u_r, u_θ) are the velocity components in the axial, radial, and azimuthal directions, and E is the total energy,

$$E = \frac{p}{\gamma - 1} + \frac{1}{2}\rho\left(u_x^2 + u_r^2 + u_\theta^2\right), \tag{4.2}$$

with the ratio of specific heats $\gamma = 1.4$ for air. It is particularly important here to note that the pressure, density, and temperature are non-dimensionalized with respect to their mean upstream values P_1, ρ_1, and T_1 respectively and are related by the ideal gas law

$$p = \rho T. \tag{4.3}$$

The velocity is scaled by the reference velocity $c^* = T_1^{1/2}$, related to the upstream mean sound speed $c_1 = \gamma^{1/2} c^*$. If M_1 is the upstream Mach number in a frame of reference in which the mean shock is stationary, then $M_1 = |U_1| / \gamma^{1/2}$. This non-dimensionalization is pertinent to our numerical experiments and will be explained later.

What was desired when the work on this problem began was to be able to show that a compelling advantage in shock mitigation and drag reduction would exist if one could suddenly deposit heat (i.e. energy) along a streamline ahead of a shockwave. To numerically study this question, the research has focused on studying axisymmetric supersonic flow over a cone. The cone approximates a vehicle in supersonic flight. With this framework in mind, the first step was to set up the global domain and divide it into appropriate sub-domains in order to be able to make use of the multi-domain WENO finite difference method. It was clear that a choice of three sub-domains was the minimum requirement. Also, since the problem is axisymmetric, it was only necessary to solve the equations in the upper half of the (x, r)-plane. The figures which follow provide a full (x, r)-plane view, but these were

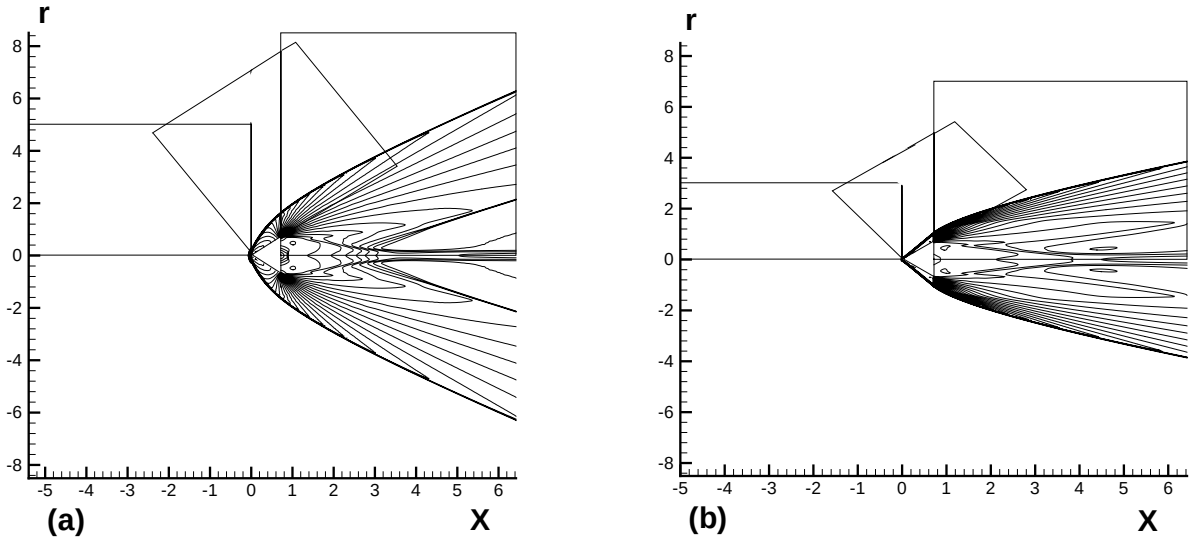

Figure 4.1: Invisicid steady state axisymmetric flow over a 45° half-angle cone is demonstrated for two different Mach numbers: (a) Mach 2, and (b) Mach 4. The computational sub-domains are indicated by the "drawn in" rectangles. Both graphs give 30 equally spaced density contours chosen appropriately to include all values computed. The results are displayed after 52000 time steps and compared visually as well as in the L_1 norm in time to ensure they indeed represent the steady state flow.

not necessary to compute. They were simply constructed from the upper half plane results using the axisymmetry.

The first step was to acquire steady state solutions of the supersonic flow over cones with varying half-angles (this is the angle made by the conical surface with the cone axis). We chose to study cones with half-angles of 45°, 30°, and 15°. Supersonic flows with Mach numbers of 2, 4, 6, and 8 were all computed. These steady state solutions were utilized as the initial conditions in the "low density core" studies. For brevity, these steady state conditions are shown only for a half-angle of 45°, in flows with Mach Numbers 2 and 4 in Figure 4.1. Note the different scales for the x and r axes.

If the sub-domains are numbered 1 through 3 from left to right respectively, the number of mesh points for the 45° half-angle cone chosen in each sub-domain was such that $\Delta x = \Delta r = \frac{1}{30}$ in sub-domain 1 and $\Delta x = \Delta r = \frac{1}{60}$ in sub-domains 2 and 3. The number of mesh points in sub-domains 2 and 3 for the 30° and 15° half-angle cones was adjusted so that

the "aspect ratio" of the interpolations at the sub-domain boundaries remained similar to that for the 45° half-angle cone. The top boundary of each sub-domain was taken to be free stream flow. The left boundary of sub-domain 1 was taken to be free inflow, and the right boundary of sub-domain 3 was taken to be free outflow. The bottom boundaries of all three of the sub-domains were reflective. This is clear for the portions of the boundaries that lie along the cone. It is also correct in axisymmetric flow with an open bottom boundary lying along the x-axis such as those of sub-domains 1 and 3. This is due to the fact that the u_r component of velocity opposes itself above and below the x-axis; whereas, the u_x and u_θ components of velocity are the same both above and below the x-axis.

Once the steady state flow initial conditions were computed, it was necessary to determine the amount of energy to deposit along the cone axis in order to open up low density cylindrical cores of various radii. Because the equations are non-dimensionalized, this was most easily determined through numerical simulation, testing different amounts of energy deposits. This energy was deposited along a line of length $5L$, where L is the length of the cone from the base to the tip. The deposited energy created low density cores of $\frac{1}{4}R$, $\frac{1}{2}R$, $\frac{3}{4}R$, and R, where R is the radius of the cone's base. It is also important to note here that because of the reflective boundary condition at the bottom of sub-domain 1 where the energy was applied, it was not truly applied along a line. This line in reality had a thickness of radius Δr because the first mesh points must be at a distance of $\frac{\Delta r}{2}$ from the line $x = 0$ in order to utilize the reflective boundary condition. It is also important to note here that the amount of energy required was indeed proportional to the square of the radius of the low density core it opened. Thus, once the amount of energy $E_{\frac{1}{4}R}$ required to open up a low density core of radius $\frac{1}{4}R$ was determined through numerical experiment, the other energy amounts were simply $4\,E_{\frac{1}{4}R}$, $9\,E_{\frac{1}{4}R}$, and $16\,E_{\frac{1}{4}R}$ respectively.

The following Figure 4.2 gives the graphical results from only one of the many numerical simulations performed. The Mach 2 results, over a cone of 45° half-angle, provide the most dramatic graphical results, and only these are presented in the interest of brevity. Each

of the steady state flows was subjected to an instantaneous line deposition of energy as described above. The deposition occurred just far enough ahead of the cone tip so that the low density cylindrical core created by this energy was open to its full radius as the front of the core reached the cone tip. Based upon a determination of how much distance would be covered by the low density core if it were traveling in a free stream flow without the cone as an obstacle, density contour snapshots were then taken at specific times. These times were selected to view the contours when 1) the leading edge of the low density core was at the cone tip; 2) the middle of the core would be at the cone tip; 3) the trailing edge of the core would be at the cone tip; and finally, 4) the core would have traveled completely past the cone by one full unit in the x-direction if it would have been in free stream flow only. Contour plots are presented in Figure 4.2 of a low density core opened to a full cone radius R in the Mach 2 flow. The contour levels were chosen appropriately to include all values of density computed.

Pressure contours will not be shown here, as they do not contribute much additional insight. It is clear from the pictured density contour plots that shock mitigation occurs. At all four Mach numbers, a comprehensive assessment was also performed of the resulting drag force on each cone shape, for each of the low density core-radii. At every time step, the drag, i.e. pressure force per unit area, on the cone was computed as:

$$D = D_{cs} - D_{cb} = 2\pi \left(\sum_{i_{cs}} \sin(\theta) r_i p_i - \sum_{j_{cb}} r_j p_j \right) \tag{4.4}$$

where D_{cs} and D_{cb} indicate the total drag along the sides of the cone and the total drag along the base of the cone respectively. θ is the cone half-angle. Because the flow is axisymmetric, only the pressure force in the x-direction is not canceled by an equal and opposite force on the opposing face of the cone. Additionally, the pressure on the base of the cone "presses" in a direction opposite to the free stream flow, thus these components subtract from the overall drag. Finally, the factor of $2\pi r$ is an approximate measure of the surface area over which that component of the drag force (pressure) is acting. Figure 4.3 shows the drag reduction that was obtained as a low density core of full cone radius R was opened ahead of a cone

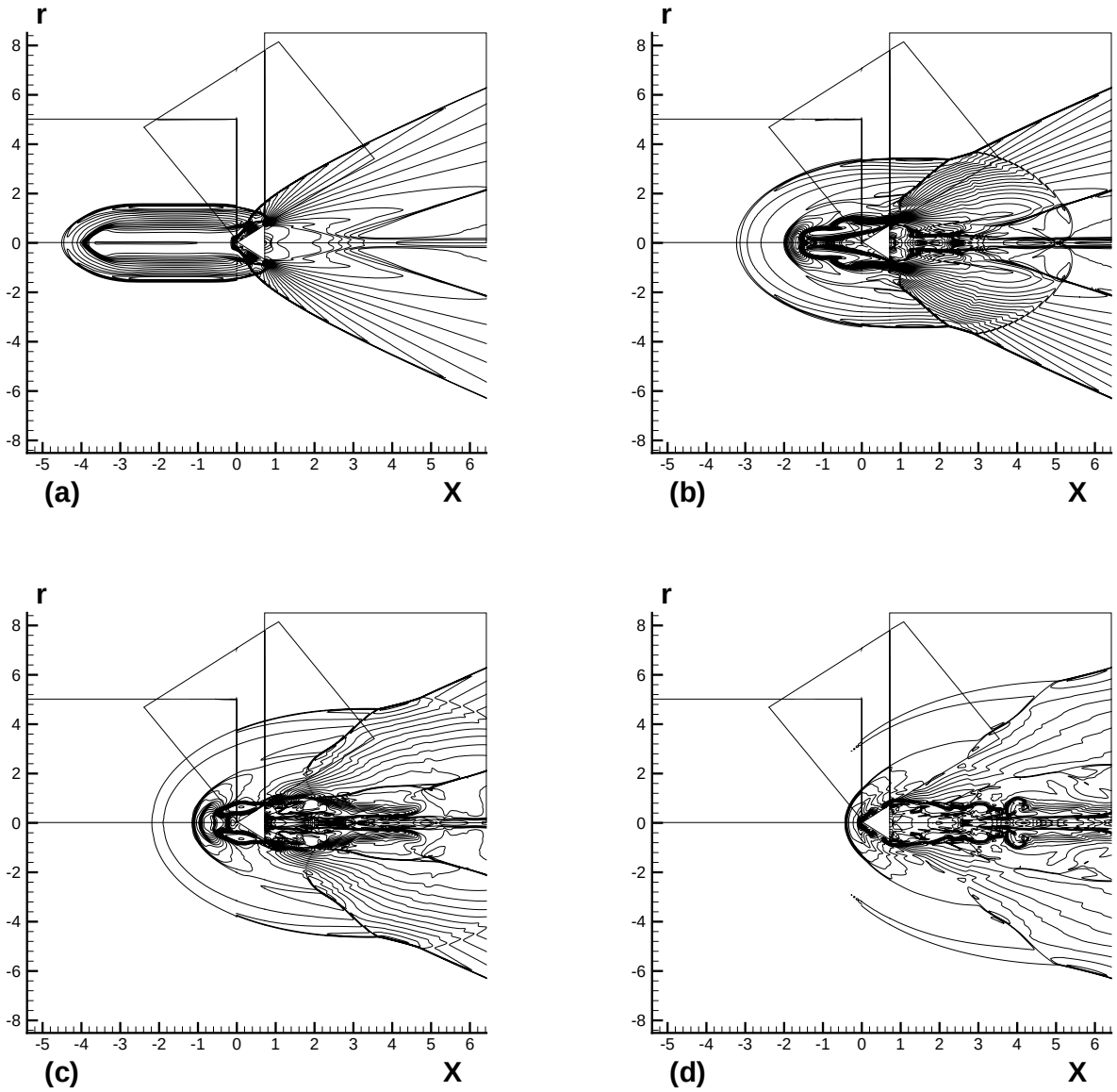

Figure 4.2: Low density core problem for Mach 2 flow over a cone. The cone half-angle is 45° over which a low density core of radius = R_{cone} is fully opened when it reaches the cone tip and remains open as it passes by the cone. The snapshots are taken at specific instants in time, namely when a) the leading edge of the low density core was at the cone tip, b) the middle of the core would be at the cone tip, c) the trailing edge of the core would be at the cone tip and d) the core would have traveled completely past the cone by one full unit in the x-direction.

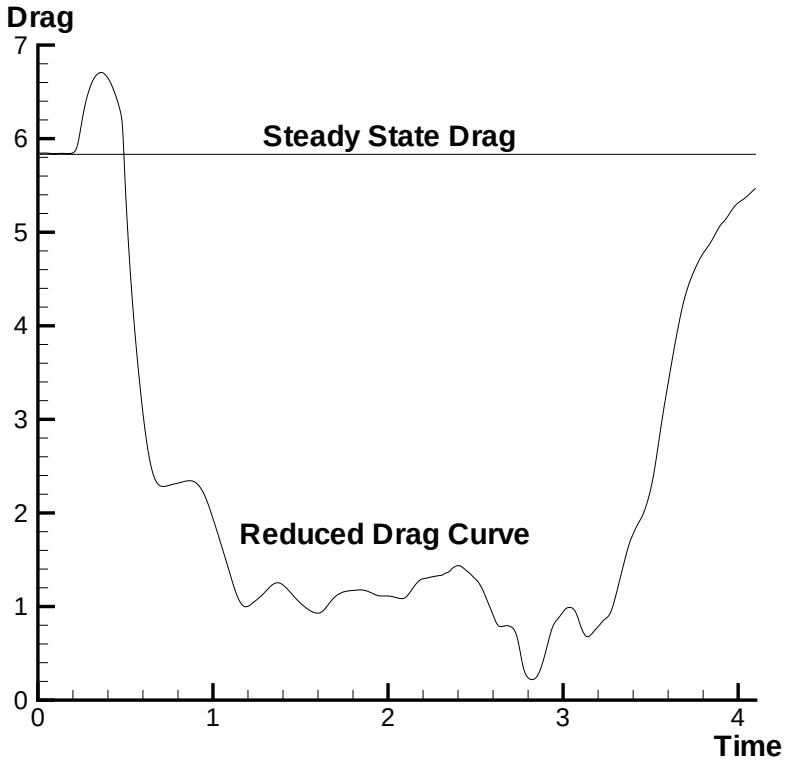

Figure 4.3: The drag reduction obtained as a cone in Mach 2 flow passes through a low density core of full cone radius R is shown. The core causes a momentary increase in drag as its expanding shock wave hits the cone; however, the drag is shown to significantly decrease for a sustained time period as the cone passes through the low density core.

in Mach 2 flow. This drag reduction graph accompanies Figure 4.2 in which four density contour plots are shown at various times as the cone passes through the low density core.

4.3 Numerical simulation summary

To facilitate comparison to experiment and theory, we chose to model the cones at zero angle of attack. For each of the different cone angles, we maintained the same base diameter. This resulted in longer cones for smaller half-angles. To obtain a more complete picture of the low density core's interaction with each cone, we always generated a heated core which was five times as long as the cone. As a result, the pertinent value, against which we show some graphs and summarizing tables, is the energy/length deposited in the flow (which is aligned

with Plooster's model).

To summarize the numerical results at a glance, Table 4.1 gives the results for the cone with 45° half-angle, Table 4.2 gives the results for the cone with 30° half-angle, and Table 4.3 gives the results for the cone with 15° half-angle.

To give a complete visual depiction of our results, the following graphs are also shown. In Figure 4.4, we plot the energy savings efficiency experienced when creating each of the four different low density cores ($\frac{1}{4}R, \frac{1}{2}R, \frac{3}{4}R, R$) in each of the supersonic flows considered (Mach 2, 4, 6, 8). Likewise, in Figure 4.5, we display the maximum drag reduction obtained when the cone passes through the low density core. "Energy Savings" is the difference between the energy expended to maintain a constant velocity with and without heating ahead of the cone. This energy expenditure is calculated by integrating the product of the drag and velocity over the amount of time that the core perturbs the steady-state flow. "Energy Savings Efficiency" is the energy savings (minus the amount of energy invested to achieve this savings) divided by the amount of energy invested to achieve this savings. Both Drag Reduction and Energy Savings Efficiency are shown as percentages to avoid confusion.

In Figure 4.6, a rough three-dimensional view of the Energy Savings Efficiency is presented. Viewing the data as a surface helps visualize the existence of potential "sweet spots", exhibiting maximal benefit. Their localized nature demonstrates the utility of mapping the "landscape" with greater resolution by performing runs at Mach numbers and energy deposition values intermediate to those already plotted.

5 Concluding remarks

Long columns of energy, deposited ahead of a vehicle, significantly reduce drag in supersonic/hypersonic regimes. The expansion of a cylindrical shockwave from the line of deposited energy results in a long, low-density column of air ahead of the vehicle. This column of low-density air interacts with the vehicle's shockwave, providing a low-density channel, along which the high pressure gas in front of the vehicle can escape, and along which the

Mach SSD	LDCR	ECC TCE	ES % ESE	LDV	% DR
2 5.845	$\frac{1}{4}$R	0.077 0.272	14.050 5074.81	1.080	81.52
	$\frac{1}{2}$R	0.307 1.086	23.510 2064.80	0.736	86.94
	$\frac{3}{4}$R	0.691 2.444	26.839 998.35	0.611	89.55
	R	1.229 4.344	28.302 551.49	0.219	96.25
4 19.615	$\frac{1}{4}$R	0.077 0.272	3.953 1355.87	17.748	9.52
	$\frac{1}{2}$R	0.307 1.086	40.735 3650.91	7.710	60.69
	$\frac{3}{4}$R	0.691 2.444	74.517 2949.49	2.786	85.80
	R	1.229 4.344	83.251 1816.38	1.669	91.49
6 41.640	$\frac{1}{4}$R	0.077 0.272	8.219 2927.07	37.429	10.11
	$\frac{1}{2}$R	0.307 1.086	37.931 3392.68	28.598	31.32
	$\frac{3}{4}$R	0.691 2.444	126.707 5085.26	6.060	85.45
	R	1.229 4.344	166.683 3736.92	2.553	93.87
8 72.395	$\frac{1}{4}$R	0.077 0.272	13.712 4950.39	65.091	10.09
	$\frac{1}{2}$R	0.307 1.086	59.674 5394.85	49.694	31.36
	$\frac{3}{4}$R	0.691 2.444	161.107 6493.02	22.964	68.28
	R	1.229 4.344	268.770 6086.88	3.750	94.82

Table 4.1: Numerical simulation results for the 45° half-angle cone. SSD is the steady state drag on the cone. LDCR is the low density core radius in terms of the radius of the base of the cone R. ECC is the non-dimensionalized energy per length required to create the core. TCE is the total amount of energy required to create the core. ES is the overall energy saved as the cone passed through the low density core and returned to steady state. %ESE is the percentage energy savings "efficiency", i.e. the ratio (in percent) of (*overall energy saved (minus the energy expended to create the core)) to (overall energy expended to create the low-density core). LDV is the lowest drag value experienced by the cone as it passed through the low density core. % DR is the percentage of drag reduction experienced with the lowest drag value as compared to the steady state drag.*

Mach SSD	LDCR	ECC TCE	ES % ESE	LDV	% DR
2 3.842	$\frac{1}{4}$R	0.077 0.470	4.844 930.00	2.861	25.54
	$\frac{1}{2}$R	0.307 1.881	15.407 719.04	1.077	71.97
	$\frac{3}{4}$R	0.691 4.232	26.967 537.17	0.827	78.49
	R	1.229 7.524	33.111 340.06	0.756	80.32
4 10.871	$\frac{1}{4}$R	0.077 0.470	4.924 946.99	9.882	9.09
	$\frac{1}{2}$R	0.307 1.881	32.750 1641.00	4.828	55.58
	$\frac{3}{4}$R	0.691 4.232	52.815 1147.88	2.565	76.40
	R	1.229 7.524	59.625 692.44	1.813	83.32
6 22.270	$\frac{1}{4}$R	0.077 0.470	8.305 1665.98	20.282	8.93
	$\frac{1}{2}$R	0.307 1.881	45.933 2341.81	13.762	38.21
	$\frac{3}{4}$R	0.691 4.232	106.668 2420.27	4.603	79.33
	R	1.229 7.524	124.857 1559.38	2.609	88.28
8 38.534	$\frac{1}{4}$R	0.077 0.470	14.661 3017.37	34.961	9.27
	$\frac{1}{2}$R	0.307 1.881	67.221 3473.47	25.294	34.36
	$\frac{3}{4}$R	0.691 4.232	178.350 4113.92	8.726	77.35
	R	1.229 7.524	212.407 2722.94	3.678	90.45

Table 4.2: Numerical simulation results for the 30° half-angle cone. SSD is the steady state drag on the cone. LDCR is the low density core radius in terms of the radius of the base of the cone R. ECC is the non-dimensionalized energy per length required to create the core. TCE is the total amount of energy required to create the core. ES is the overall energy saved as the cone passed through the low density core and returned to steady state. %ESE is the percentage energy savings "efficiency", i.e. the ratio (in percent) of (*overall energy saved (minus the energy expended to create the core)) to (overall energy expended to create the low-density core). LDV is the lowest drag value experienced by the cone as it passed through the low density core. % DR is the percentage of drag reduction experienced with the lowest drag value as compared to the steady state drag.*

Mach SSD	LDCR	ECC TCE	ES % ESE	LDV	% DR
2 1.731	$\frac{1}{4}$R	0.077 1.013	1.792 76.87	1.562	9.77
	$\frac{1}{2}$R	0.307 4.053	6.217 53.38	1.040	39.93
	$\frac{3}{4}$R	0.691 9.120	12.923 41.70	0.588	66.04
	R	1.229 16.213	16.341 0.79	0.344	80.15
4 3.800	$\frac{1}{4}$R	0.077 1.013	2.725 168.91	3.523	7.28
	$\frac{1}{2}$R	0.307 4.053	15.535 283.28	2.392	37.05
	$\frac{3}{4}$R	0.691 9.120	24.713 170.99	1.717	54.82
	R	1.229 16.213	30.613 88.82	1.223	67.83
6 6.460	$\frac{1}{4}$R	0.077 1.013	5.257 418.81	5.885	8.90
	$\frac{1}{2}$R	0.307 4.053	29.859 636.68	3.593	44.38
	$\frac{3}{4}$R	0.691 9.120	48.692 433.93	2.085	67.73
	R	1.229 16.213	58.473 260.66	1.254	80.59
8 10.447	$\frac{1}{4}$R	0.077 1.013	8.803 768.77	9.471	9.34
	$\frac{1}{2}$R	0.307 4.053	39.057 864.64	6.501	37.77
	$\frac{3}{4}$R	0.691 9.120	90.126 888.26	2.933	71.93
	R	1.229 16.213	103.846 540.53	1.506	85.58

Table 4.3: Numerical simulation results for the 15° half-angle cone. SSD is the steady state drag on the cone. LDCR is the low density core radius in terms of the radius of the base of the cone R. ECC is the non-dimensionalized energy per length required to create the core. TCE is the total amount of energy required to create the core. ES is the overall energy saved as the cone passed through the low density core and returned to steady state. %ESE is the percentage energy savings "efficiency", i.e. the ratio (in percent) of (*overall energy saved (minus the energy expended to create the core)) to (overall energy expended to create the low-density core). LDV is the lowest drag value experienced by the cone as it passed through the low density core. % DR is the percentage of drag reduction experienced with the lowest drag value as compared to the steady state drag.*

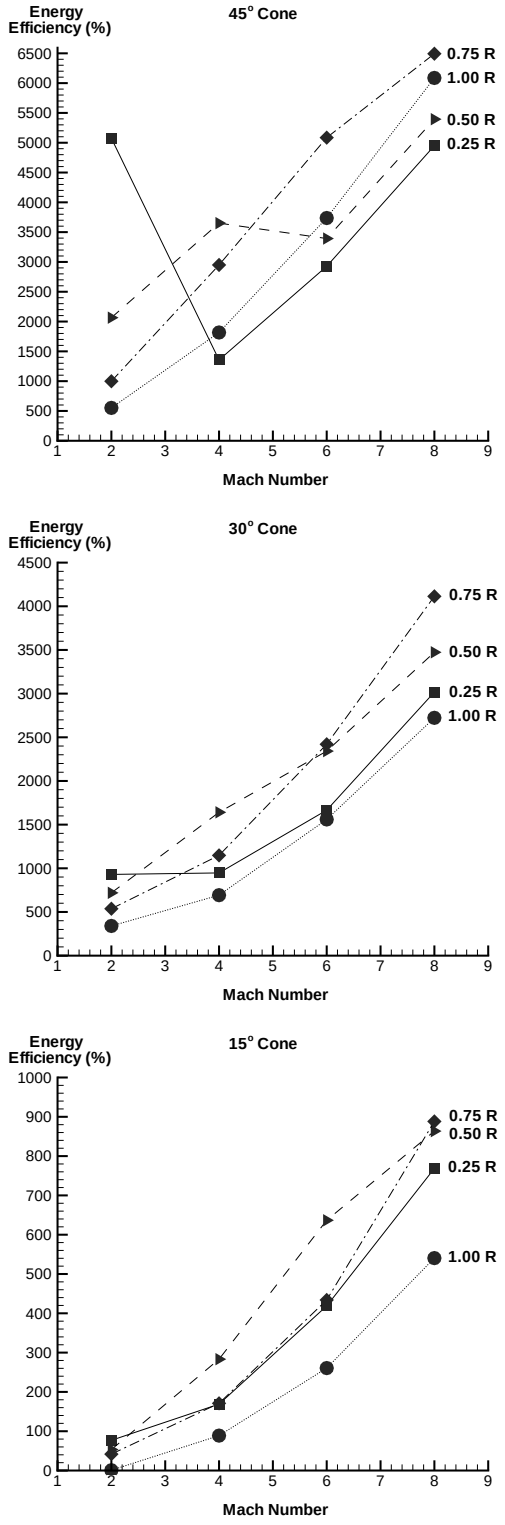

Figure 4.4: Display of the overall energy savings efficiency percentage of creating a low density core for each of the supersonic flows computed, and each of the cores created.

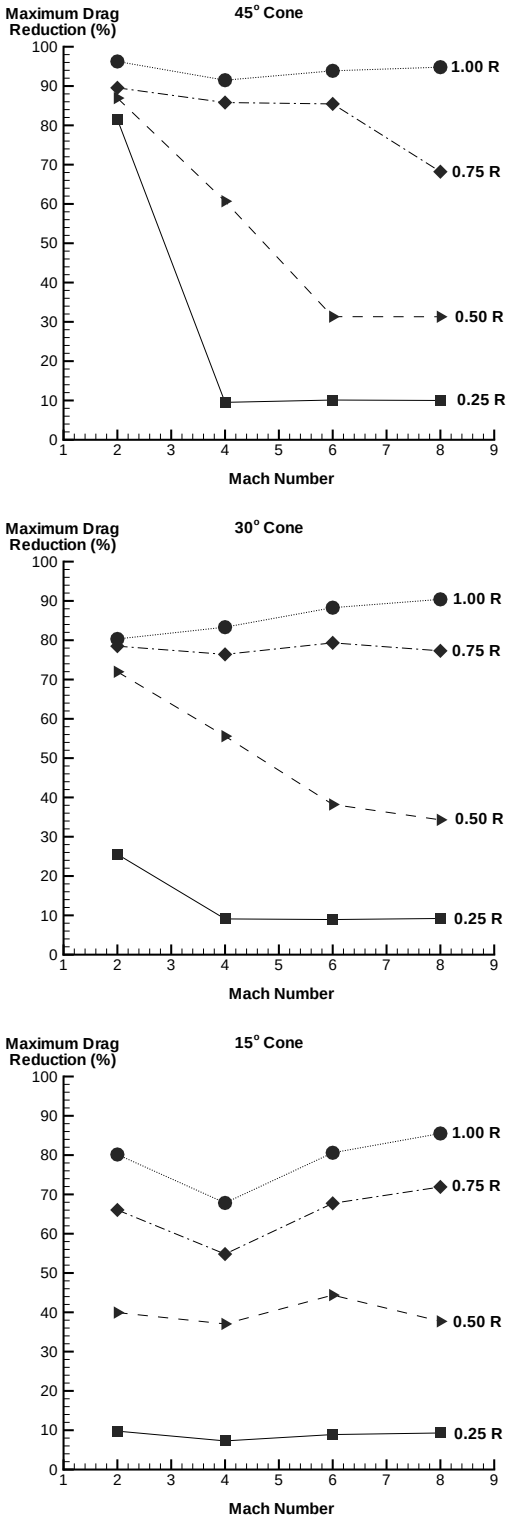

Figure 4.5: Display of the maximum drag reduction percentage as a result of creating a low density core for each of the supersonic flows computed, and each of the cores created.

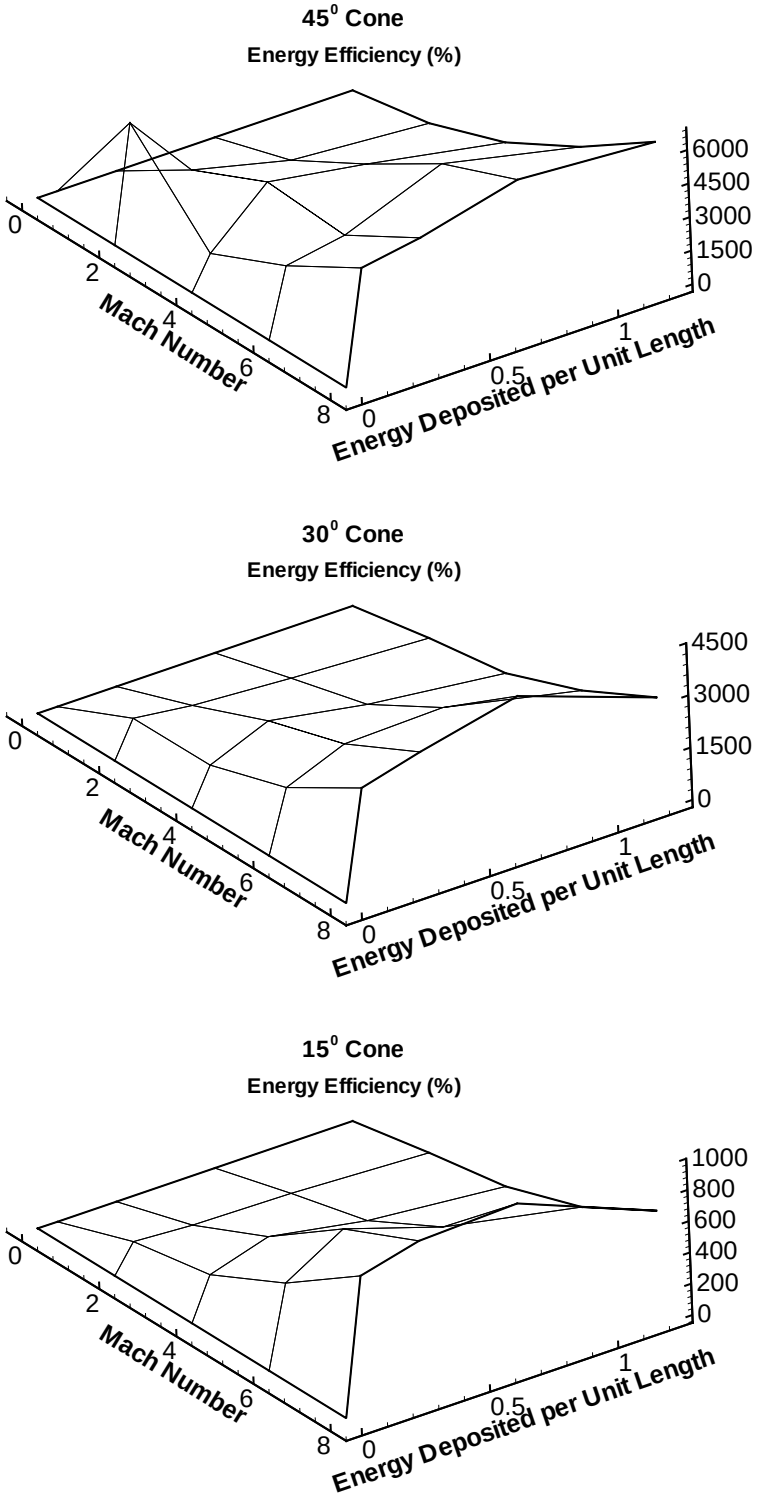

Figure 4.6: Three dimensional views of the overall energy savings efficiency (as a percentage) obtained for the three cone half-angles.

vehicle can travel with greatly reduced wave drag. Having compared this method to energy-deposition at a "point" ahead of the shock wave, we have numerically demonstrated a far greater benefit for deposition along lines which are aligned with the vehicle's direction of motion.

As much as a 96% reduction in drag was observed as a direct result of the energy deposition. The drag reduction is also economically favorable, with a "return on invested energy" as high as 6500%. Different amounts of deposited energy (yielding different radii low-density columns) yield the highest energy efficiency for different Mach numbers and cone half-angles.

Our next step in the supersonic/hypersonic regimes will be to experimentally demonstrate and characterize the described method in a clean wind tunnel with excellent high-resolution diagnostics. Experimental data on cones will allow us to further validate our computational methods, which can then be used to investigate optimized vehicle designs and to make scale models for further testing and advances in our wind tunnel experiments. Additional areas for future investigation are to:

- Explore optimal geometry and frequency of energy deposition for flow control and drag reduction.
- Use energy deposition to mitigate an adverse flow condition, as well as reduce drag.
- Develop dynamic, data-driven control for energy deposition to optimize drag reduction and shock mitigation.
- Include Navier-Stokes terms, which will improve drag-reduction yet further, because of the temperature-dependence of the viscous drag.

References

[1] R.G. Adelgren, G.S. Elliot, D.D. Knight, A.A. Zheltovodov and T.J. Beutner, *Energy deposition in supersonic flows*, AIAA Paper 2001-0885.

[2] Aleksandrov, N. Vidyakin, V. Lakutin et al., *On a possible mechanism of interaction of a shock wave with the decaying plasma of a laser spark in air*, Zhurnal Tekhnika Fizika, v56 (1986), p.771.

[3] D. Balsara and C.-W. Shu, *Monotonicity preserving weighted essentially non-oscillatory schemes with increasingly high order of accuracy*, J. Comput. Phys., v160 (2000), pp.405-452.

[4] V. Bityurin, A. Klimov, S. Leonov, N. Popov and D. Van Wie, *Shock wave structure and velocity at propagation through non-homogeneous plasma*, AIAA Paper 2000-2571.

[5] P. Bletzinger, B.N. Ganguly and A. Garscadden, *Mutual interactions between low Mach number shock waves and nonequilibrium plasmas*, AIAA Paper 2001-3050.

[6] A. Brodeur, C.Y. Chien, F.A. Ilkov, S.L. Chin, O.G. Kosareva and V.P. Kandidov, *Moving focus in the propagation of ultrashort laser pulses in air*, Optics Letters, v22 (1997), pp.304-306.

[7] J.-C. Diels et al. *Tests of laser-induced discharge of high DC voltage using high-power femtosecond UV pulses*, Proceedings of Advanced High-Power Lasers and Applications, Osaka, Nov 1999.

[8] O. Friedrichs, *Weighted essentially non-oscillatory schemes for the interpolation of mean values on unstructured grids*, J. Comput. Phys., v144 (1998), pp.194–212.

[9] B.N. Ganguly, P. Bletzinger and A. Garscadden, *Shock wave damping and dispersion in nonequilibrium low pressure argon plasmas*, Physics Letters A 230, 1997, pp.218-222.

[10] Y. Guy, T.E. McLaughlin and J.A. Morrow, *Blunt body wave reduction by means of a standoff spike*, AIAA Paper 2001-0888.

[11] A. Harten, B. Engquist, S. Osher and S. Chakravarthy, *Uniformly high order essentially non-oscillatory schemes, III*, J. Comput. Phys., v71 (1987), pp.231–303.

[12] C. Hu and C.-W. Shu, *Weighted essentially non-oscillatory schemes on triangular meshes*, J. Comput. Phys., v150 (1999), pp.97-127.

[13] Y.K. Ionikh, N.V. Chernysheva, A.P. Yalin, S.O. Macharet, L. Martinelli and R.B. Miles, AIAA Paper 2000–0714.

[14] G. Jiang and C.-W. Shu, *Efficient implementation of weighted ENO schemes*, J. Comput. Phys., v126 (1996), pp.202–228.

[15] S.W. Kandebo, *"Air spike" could ease hypersonic flight problems*, Aviation Week and Space Technology, May 1995, p.65.

[16] A.I. Klimov, A.N. Koblov, G.I. Mishin, Yu. L. Serov and I.P. Yavor, Soviet Tech. Phys. Lett. 8 (4), 8 (5), 1982, pp.192-194, 240-241.

[17] K. Kremeyer, S. Nazarenko and A. Newell, *The effect of fore-shock heating in the plasma drag-reduction problem*, AIAA Paper 2000-2700.

[18] K. Kremeyer, S. Nazarenko and A. Newell, Presentation at the co-sponsored AIAA/AFOSR Weakly Ionized Gases, Space-Planes, and Hypersonics Meeting, Norfolk, 1998.

[19] K. Kremeyer, S. Nazarenko and A. Newell, *The role of vorticity in shock propagation through inhomogeneous media*, AIAA Paper 99-0871.

[20] K. Kremeyer, S. Nazarenko and A. Newell, *Shock bowing and vorticity dynamics during propagation into different transverse density profiles*, Physica D, v163 (2002), pp.150-165.

[21] K. Kremeyer, USPTO, patent number 6,527,221 B1, May 2000.

[22] B. La Fontaine, F. Vidal, Z. Jiang, C.Y. Chien, D. Comtois, A. Desparois, T.W. Johnston, J.-C. Kieffer, H. Pepin and H.P. Mercure, *Filamentation of ultrashort pulse laser*

beams resulting from their propagation over long distances in air, Physics of Plasmas, v6 (1999), pp. 1615-1621.

[23] X.-D. Liu, S. Osher and T. Chan, *Weighted essentially non-oscillatory schemes*, J. Comput. Phys., v115 (1994), pp.200–212.

[24] M. Lutzky and D.L. Lehto, *Shock propagation in spherically symmetric exponential atmospheres*, Physics of Fluids, v11 (1968), pp.1466-1472.

[25] S. Merriman, A. Christian, R. Meyer, B. Kowalczyk, P. Palm and I. Adamovich, *Studies of conical shockwave modification by nonequilibrium RF discharge plasma*, AIAA Paper 2001-0347.

[26] L.N. Myrabo and Y. Raizer, *Laser-induced air spike for advanced transatmospheric vehicles*, AIAA Paper 94-2451.

[27] M.N. Plooster, *Shock waves from line sources, numerical solutions and experimental measurements*, Phys. Fluids, v13 (1970), pp.2665-2675.

[28] P. Rambo, J. Schwarz and J.-C. Diels, *High-voltage electrical discharges induced by an ultrashort-pulse UV laser system*, J. Opt. A: Pure Appl. Opt. 3 (2001), pp.146-158.

[29] D. Riggins, H.F. Nelson and E. Johnson, *Blunt-body wave drag reduction using focused energy deposition*, AIAA Journal, v37 (1999), pp.460-467.

[30] P.L. Sachdev, *Propagation of a blast wave in uniform or non-uniform media: a uniformly valid analytic solution*, J. Fluid Mech., v52 (1972), pp.369-378.

[31] S. Schreier, *Compressible Flow*, John Wiley and Sons Inc., New York, 1982.

[32] J. Schwarz, P.K. Rambo and J.-C. Diels, *Comparative observations of filaments at 248nm and 800 nm*, Submitted to Optics Communications.

[33] J. Schwarz and J.-C. Diels, *Long distance propagation of UV filaments*, Journal of Modern Optics, v49 (2002), pp.2583-2597.

[34] K. Sebastian and C.-W. Shu, *Multi domain WENO finite difference method with interpolation at sub-domain interfaces*, J. Sci. Comput., v19 (2003), pp.405-438.

[35] J. Shang, AFRL/WPAFB, AIAA Presentation

[36] J. Shi, C. Hu and C.-W. Shu, *A technique of treating negative weights in WENO schemes*, J. Comput. Phys., v175 (2002), pp.108-127.

[37] Y.N. Yudintsev and V.F. Chirkashenko, *Modes of counterjet interaction with a supersonic flow*, Gas Dynamics and Acoustics of Jet Flows, 1979, pp.75-107, Novosibirsk (in Russian).